

NUMERICAL APPROXIMATION OF VISCOELASTIC FLUID-STRUCTURE INTERACTION PROBLEMS

HYESUK LEE AND SHUHAN XU

(Communicated by T. Iliescu)

Dedicated to Professor William J. Layton on the occasion of his 60th birthday

Abstract. We consider a fluid-structure interaction (FSI) problem that consists of a viscoelastic fluid flow and a linear elastic structure. The system is formulated as (i) a monolithic problem, where the matching conditions at the moving interface are satisfied implicitly, and (ii) a partitioned problem, where the fluid and structure subproblems are coupled by Robin-type boundary conditions along the interface. Numerical algorithms are designed based on the Arbitrary Lagrangian-Eulerian (ALE) formulation for the time-dependent fluid domain. We perform numerical experiments to compare monolithic and partitioned schemes and study the effect of stress boundary conditions on the inflow portion of moving interface.

Key words. Fluid-structure interaction, viscoelastic fluid.

1. Introduction

Fluid-structure interaction (FSI) problems are multi-physics problems involving fluid flows and deformable structures. Such problems are widely used in engineering and biological applications where a surrounding or internal fluid interacts with a movable structure. In general, such FSI problems are solved by either a monolithic or a partitioned approach. The monolithic approach solves the entire problem within one complex system considering fluid and structure together while treating the interface conditions implicitly. The partitioned approach, on the other hand, decouples the interaction system into two subproblems and uses local solvers. The interface-matching conditions are explicit as a bridge of the two subproblems. A monolithic algorithm requires a large memory storage and a special solver, but avoids the stability issue existing in many partitioned algorithms. When densities of the fluid and structure are close, explicit staggered approaches often fail and even implicit staggered methods may become unstable due to the added mass effect [8, 13, 16, 18, 30].

Much work has been done with both monolithic and partitioned approaches for Newtonian FSI problems where the fluid viscosity is constant. Fluids of interest in some FSI problems include blood, air in the bronchial passages, paint, latex, and other industrial polymers. There are some difficulties of simulating a fluid which is non-Newtonian in nature since the shear stress of fluid is not proportional to the shear rate. In simulations of blood flow, Newtonian models have been used and have performed well in most cases where a larger vessel is considered such as the aorta. However, it is well known that blood flow through small caliber vessels shows non-Newtonian behavior, therefore demanding a more accurate and realistic model [2, 4, 5, 15, 19, 21, 25, 28, 29].

Unlike Newtonian FSI, which have been thoroughly elucidated [6, 7, 11, 12], few analytical and numerical studies have been undertaken for interaction of non-Newtonian fluids and elastic solids. Shear-thinning viscoelastic fluid models are presented and numerically tested for a blood flow in [3, 5]. Chan et al. considered Carreau fluid and power law fluid for FSI problems and compared the numerical results of the two different fluid models [9]. An energy estimate and numerical results using a splitting method is presented by J.Janela et al. for a generalized Newtonian shear-thinning FSI problem [19], and an extended study was performed by the same authors for several absorbing boundary conditions [20]. Relevant numerical studies considering a viscoelastic flow through a flexible channel were done by Chen et al. [10], and a mass-spring-dashpot prototype model was also examined by the same authors. In our recent work [23, 24], we have analyzed quasi-Newtonian FSI problems for stability and finite element error estimates.

In this paper, we consider a viscoelastic fluid where a separate hyperbolic differential constitutive equation is required to describe the complicated stress-deformation relation. Difficulties arise from both analytical and computational aspects due to the hyperbolic character and the lack of a stabilizing term for the stress. It is well known that for a viscoelastic fluid, a stress boundary condition on the inflow boundary must be imposed to ensure the well-posedness of the model equations. When a partitioned scheme is considered for simulating viscoelastic FSI, an extra difficulty is encountered due to (i) the movement of inlet and outlet boundaries along the interface of two substructures and (ii) the lack of information on the stress along the moving boundary. There are a few studies on viscoelastic FSI problems by partitioned methods in the literature [3, 5, 10]; however, no numerical methods or discussion have been reported to handle stress boundary conditions on the interface. In this work, we simulate the viscoelastic FSI problem using a monolithic and a partitioned algorithm and investigate how the stress boundary condition affects the FSI system.

The paper is organized as follows. Section 2 introduces model equations of the fluid-structure system with initial and boundary conditions. The matching conditions for the two dynamics on the interface are also provided in this section. In Section 3, we provide a monolithic and a partitioned formulation in the ALE framework. The last section presents numerical experiments and comparison of numerical results by algorithms discussed in Section 3.

2. Models Equations and Framework

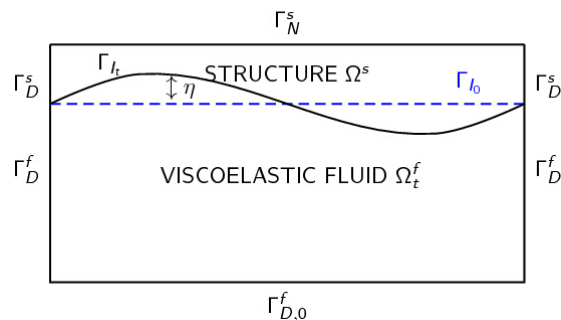


FIGURE 1. Fluid-Structure interaction domain.

The FSI system considered consists of a viscoelastic fluid and an isotropic linear elastic structure as shown in Figure 1. Let Ω_t^f be the moving fluid domain at t in \mathbb{R}^d , $d = 2, 3$, with the boundary $\Gamma_t^f := \Gamma_{D,0}^f \cup \Gamma_D^f \cup \Gamma_{I_t}$, where Γ_{I_t} is the moving interface boundary. Let Ω^s be a fixed domain for the structure described in terms of the Lagrangian frame of reference. The boundary of the structure is denoted as $\Gamma_t^s := \Gamma_N^s \cup \Gamma_D^s \cup \Gamma_{I_t}$.

We consider the FSI system where the fluid equations are given by the Johnson-Segalman viscoelastic model equations

$$(1) \quad \boldsymbol{\sigma} + \lambda \left(\frac{\partial \boldsymbol{\sigma}}{\partial t} + \mathbf{u} \cdot \nabla \boldsymbol{\sigma} + g_\beta(\boldsymbol{\sigma}, \nabla \mathbf{u}) \right) - 2\alpha D(\mathbf{u}) = \mathbf{0} \quad \text{in } \Omega_t^f,$$

$$(2) \quad \rho_f \left(\frac{\partial \mathbf{u}}{\partial t} + \mathbf{u} \cdot \nabla \mathbf{u} \right) - \nabla \cdot \boldsymbol{\sigma} - 2(1 - \alpha) \nabla \cdot D(\mathbf{u}) + \nabla p = \mathbf{f}_f \quad \text{in } \Omega_t^f,$$

$$(3) \quad \nabla \cdot \mathbf{u} = 0 \quad \text{in } \Omega_t^f,$$

where $\boldsymbol{\sigma}$ denotes the extra stress tensor, \mathbf{u} the velocity vector, p the pressure of fluid, Re the Reynolds number, and λ is the Weissenberg number defined as the product of the relaxation time and a characteristic strain rate. In (1) and (2), $D(\mathbf{u}) := (\nabla \mathbf{u} + \nabla \mathbf{u}^T)/2$ is the rate of the strain tensor, α is a number such that $0 < \alpha < 1$ which may be considered to be the fraction of viscoelastic viscosity, and \mathbf{f} is the body force. In (1), $g_\beta(\boldsymbol{\sigma}, \nabla \mathbf{u})$ is defined by

$$(4) \quad g_\beta(\boldsymbol{\sigma}, \nabla \mathbf{u}) := \frac{1 - \beta}{2} (\boldsymbol{\sigma} \nabla \mathbf{u} + \nabla \mathbf{u}^T \boldsymbol{\sigma}) - \frac{1 + \beta}{2} (\nabla \mathbf{u} \boldsymbol{\sigma} + \boldsymbol{\sigma} \nabla \mathbf{u}^T)$$

for $\beta \in [-1, 1]$. Note that (1) reduces to the Oldroyd-B model for the case $\beta = 1$. The structure is described by an isotropic linear elastic structure as

$$(5) \quad \rho_s \frac{\partial^2 \boldsymbol{\eta}}{\partial t^2} - 2\nu_s \nabla \cdot D(\boldsymbol{\eta}) - \bar{\lambda} \nabla (\nabla \cdot \boldsymbol{\eta}) = \mathbf{f}_s \quad \text{in } \Omega^s,$$

where $\boldsymbol{\eta}$ is the displacement of structure and ρ_s and \mathbf{f}_s are the density and body force of the structure, respectively. ν_s and λ are the Lamé parameters defined as

$$(6) \quad \nu_s = \frac{E}{2(1+r)}, \quad \bar{\lambda} = \frac{rE}{(1-2r)(1+r)},$$

where E is the Young's Modulus of the structure and r is its Poisson ratio.

Initial and boundary conditions for \mathbf{u} and $\boldsymbol{\sigma}$ are given as follows:

$$(7) \quad \mathbf{u}(\mathbf{x}, 0) = \mathbf{u}_0, \quad \boldsymbol{\sigma}(\mathbf{x}, 0) = \boldsymbol{\sigma}_0 \quad \text{in } \Omega_0^f,$$

$$(8) \quad \boldsymbol{\eta}(\mathbf{x}, 0) = \boldsymbol{\eta}_0, \quad \boldsymbol{\eta}_t(\mathbf{x}, 0) = \dot{\boldsymbol{\eta}}_0 \quad \text{in } \Omega^s,$$

$$(9) \quad \mathbf{u} = \mathbf{u}_D \quad \text{on } \Gamma_D^f,$$

$$(10) \quad \mathbf{u} = \mathbf{0} \quad \text{on } \Gamma_{D,0}^f,$$

$$(11) \quad \boldsymbol{\sigma} = \boldsymbol{\sigma}_D \quad \text{on } \Gamma_{inlet}^f,$$

$$(12) \quad 2\nu_s \mathbf{D}(\boldsymbol{\eta}) \mathbf{n}_s + \bar{\lambda} (\nabla \cdot \boldsymbol{\eta}) \mathbf{n}_s = \mathbf{0} \quad \text{on } \Gamma_N^s,$$

$$(13) \quad \boldsymbol{\eta} = \mathbf{0} \quad \text{on } \Gamma_D^s.$$

In (11) Γ_{inlet}^f is a portion of Γ_D^f , where the normal velocity of fluid is negative. The moving interface Γ_{I_t} is determined by the displacement $\boldsymbol{\eta}$ at time t . Based on

the continuity of the velocity and the stress force, the matching conditions on the interface are

$$(14) \quad \frac{\partial \boldsymbol{\eta}}{\partial t} = \mathbf{u} \quad \text{on } \Gamma_{I_t},$$

$$(15) \quad (\boldsymbol{\sigma} + 2(1 - \alpha)D(\mathbf{u}) - p\mathbf{I})\mathbf{n}_f = -(2\nu_s D(\boldsymbol{\eta}) + \bar{\lambda}(\nabla \cdot \boldsymbol{\eta}))\mathbf{n}_s \quad \text{on } \Gamma_{I_t},$$

where \mathbf{n}_f and \mathbf{n}_s are the outward unit normal vectors to Ω_t^f and Ω^s , respectively.

For any time $t \in (0, T]$, we define a bijective mapping Ψ_t which maps the reference domain Ω_0^f to the physical domain Ω_t^f ,

$$(16) \quad \Psi_t : \Omega_0^f \rightarrow \Omega_t^f, \quad \Psi_t(\mathbf{y}) = \mathbf{x}(t, \mathbf{y}),$$

where \mathbf{x} and \mathbf{y} are the spatial coordinates in Ω_t^f and Ω_0^f , respectively. We refer to \mathbf{x} as the Eulerian coordinate and \mathbf{y} as the Arbitrary Lagrangian Eulerian (ALE) coordinate. The ALE formulation for (1)-(5) is then given by

$$(17) \quad \boldsymbol{\sigma} + \lambda \left(\frac{\partial \boldsymbol{\sigma}}{\partial t} \Big|_{\mathbf{y}} + (\mathbf{u} - \mathbf{z}) \cdot \nabla_{\mathbf{x}} \boldsymbol{\sigma} + g_{\beta}(\boldsymbol{\sigma}, \nabla_{\mathbf{x}} \mathbf{u}) \right) - 2\alpha D_{\mathbf{x}}(\mathbf{u}) = \mathbf{0} \quad \text{in } \Omega_t^f,$$

$$(18) \quad Re \left(\frac{\partial \mathbf{u}}{\partial t} \Big|_{\mathbf{y}} + (\mathbf{u} - \mathbf{z}) \cdot \nabla_{\mathbf{x}} \mathbf{u} \right) - \nabla_{\mathbf{x}} \cdot \boldsymbol{\sigma} - 2(1 - \alpha) \nabla_{\mathbf{x}} \cdot D_{\mathbf{x}}(\mathbf{u}) \\ + \nabla_{\mathbf{x}} p = \mathbf{f}_f \quad \text{in } \Omega_t^f,$$

$$(19) \quad \nabla_{\mathbf{x}} \cdot \mathbf{u} = 0 \quad \text{in } \Omega_t^f,$$

$$(20) \quad \rho_s \frac{\partial^2 \boldsymbol{\eta}}{\partial t^2} - 2\nu_s \nabla \cdot D(\boldsymbol{\eta}) - \bar{\lambda} \nabla \cdot (\nabla \cdot \boldsymbol{\eta}) = \mathbf{f}_s \quad \text{in } \Omega^s,$$

where $\mathbf{z} := \frac{\partial \mathbf{x}}{\partial t} \Big|_{\mathbf{y}}$ is the domain velocity and $\frac{\partial \boldsymbol{\sigma}}{\partial t} \Big|_{\mathbf{y}}, \frac{\partial \mathbf{u}}{\partial t} \Big|_{\mathbf{y}}$ are the ALE derivatives of $\boldsymbol{\sigma}$ and \mathbf{u} , respectively. See [23, 24] for details.

Define the function spaces

$$\mathbf{U}_0 := \{\bar{\mathbf{v}} \in \mathbf{H}^1(\Omega_0^f) : \bar{\mathbf{v}} = \mathbf{0} \quad \text{on } \Gamma_D^f \cup \Gamma_{D,0}^f\},$$

$$Q_0 := L^2(\Omega_0^f),$$

$$\boldsymbol{\Sigma}_0 := \{\bar{\boldsymbol{\tau}} \in \mathbf{L}^2(\Omega_0^f) : \bar{\tau}_{ij} = \bar{\tau}_{ji}, \bar{\boldsymbol{\tau}} = \mathbf{0}\},$$

$$\mathbf{U}_t := \{\mathbf{v} : \mathbf{v} = \bar{\mathbf{v}} \circ \Psi_t^{-1} \text{ for } \bar{\mathbf{v}} \in \mathbf{U}_0\},$$

$$Q_t := \{q : q = \bar{q} \circ \Psi_t^{-1} \text{ for } \bar{q} \in Q_0\},$$

$$\boldsymbol{\Sigma}_t := \{\boldsymbol{\tau} : \boldsymbol{\tau} = \bar{\boldsymbol{\tau}} \circ \Psi_t^{-1} \text{ for } \bar{\boldsymbol{\tau}} \in \boldsymbol{\Sigma}_0\},$$

$$\mathbf{S} := \{\boldsymbol{\xi} \in \mathbf{H}^1(\Omega^s) : \boldsymbol{\xi} = \mathbf{0} \quad \text{on } \Gamma_D^s\}.$$

Using Reynolds transport theorem

$$(21) \quad \left(\frac{\partial \phi}{\partial t} \Big|_{\mathbf{y}}, v \right)_{\Omega_t^f} = \frac{d}{dt} (\phi, v)_{\Omega_t^f} - (\phi \nabla_{\mathbf{x}} \cdot \mathbf{z}, v)_{\Omega_t^f},$$

we obtain the variational formulation of the FSI system: find $(\mathbf{u}, p, \boldsymbol{\sigma}, \boldsymbol{\eta})$ satisfying (9), (11) and

$$(22) \quad (\boldsymbol{\sigma}, \boldsymbol{\tau})_{\Omega_t^f} + \lambda \frac{d}{dt} (\boldsymbol{\sigma}, \boldsymbol{\tau})_{\Omega_t^f} + \lambda (-\boldsymbol{\sigma}(\nabla_{\mathbf{x}} \cdot \mathbf{z}) + ((\mathbf{u} - \mathbf{z}) \cdot \nabla_{\mathbf{x}}) \boldsymbol{\sigma}, \boldsymbol{\tau})_{\Omega_t^f} \\ + \lambda (g_\beta(\boldsymbol{\sigma}, \nabla_{\mathbf{x}} \mathbf{u}), \boldsymbol{\tau})_{\Omega_t^f} - 2\alpha (D_{\mathbf{x}}(\mathbf{u}), \boldsymbol{\tau})_{\Omega_t^f} = \mathbf{0} \quad \forall \boldsymbol{\tau} \in \boldsymbol{\Sigma}_t,$$

$$(23) \quad Re \frac{d}{dt} (\mathbf{u}, \mathbf{v})_{\Omega_t^f} + Re (-\mathbf{u}(\nabla_{\mathbf{x}} \cdot \mathbf{z}) + (\mathbf{u} - \mathbf{z}) \cdot \nabla_{\mathbf{x}} \mathbf{u}, \mathbf{v})_{\Omega_t^f} + (\boldsymbol{\sigma}, D_{\mathbf{x}}(\mathbf{v}))_{\Omega_t^f} \\ + 2(1 - \alpha)(D_{\mathbf{x}}(\mathbf{u}), D_{\mathbf{x}}(\mathbf{v}))_{\Omega_t^f} - (p, \nabla_{\mathbf{x}} \cdot \mathbf{v})_{\Omega_t^f} \\ = (\mathbf{f}, \mathbf{v})_{\Omega_t^f} + ((\boldsymbol{\sigma} + 2(1 - \alpha) D_{\mathbf{x}}(\mathbf{u}) - pI) \mathbf{n}_f, \mathbf{v})_{\Gamma_{I_t}} \quad \forall \mathbf{v} \in \mathbf{U}_t,$$

$$(24) \quad (q, \nabla_{\mathbf{x}} \cdot \mathbf{u})_{\Omega_t^f} = 0 \quad \forall q \in Q_t,$$

$$(25) \quad \rho_s \left(\frac{\partial^2 \boldsymbol{\eta}}{\partial t^2}, \boldsymbol{\xi} \right) + 2\nu_s (D(\boldsymbol{\eta}), D(\boldsymbol{\xi})) + \bar{\lambda} (\nabla \cdot \boldsymbol{\eta}, \nabla \cdot \boldsymbol{\xi}) \\ = (\mathbf{f}_s, \boldsymbol{\xi}) + ((2\nu_s D(\boldsymbol{\eta}) + \bar{\lambda} (\nabla \cdot \boldsymbol{\eta})) \mathbf{n}_s, \boldsymbol{\xi})_{\Gamma_{I_0}} \quad \forall \boldsymbol{\xi} \in \mathbf{S}.$$

By introducing the coupled test function space

$$\tilde{\mathbf{U}}_t \times \tilde{\mathbf{S}} := \{(\mathbf{v}, \boldsymbol{\xi}) \in \mathbf{U}_t \times \mathbf{S} : \mathbf{v}|_{\Gamma_{I_t}} = \left(\frac{\partial \boldsymbol{\xi}}{\partial t} \circ \Psi_t^{-1} \right) |_{\Gamma_{I_t}}\}$$

and using (15), the monolithic scheme of the weak formulation is written as

$$(26) \quad \rho_s \left(\frac{\partial^2 \boldsymbol{\eta}}{\partial t^2}, \boldsymbol{\xi} \right)_{\Omega^s} + 2\nu_s (\mathbf{D}(\boldsymbol{\eta}), \mathbf{D}(\boldsymbol{\xi}))_{\Omega^s} + \bar{\lambda} (\nabla \cdot \boldsymbol{\eta}, \nabla \cdot \boldsymbol{\xi})_{\Omega^s} \\ + \lambda \left[\frac{d}{dt} (\boldsymbol{\sigma}, \boldsymbol{\tau})_{\Omega_t^f} - (\boldsymbol{\sigma}(\nabla_{\mathbf{x}} \cdot \mathbf{z}), \boldsymbol{\tau})_{\Omega_t^f} + (((\mathbf{u} - \mathbf{z}) \cdot \nabla_{\mathbf{x}}) \boldsymbol{\sigma}, \boldsymbol{\tau})_{\Omega_t^f} \right. \\ \left. + (g_\beta(\boldsymbol{\sigma}, \nabla_{\mathbf{x}} \mathbf{u}), \boldsymbol{\tau})_{\Omega_t^f} \right] \\ + Re \left[\frac{d}{dt} (\mathbf{u}, \mathbf{v})_{\Omega_t^f} - (\mathbf{u}(\nabla_{\mathbf{x}} \cdot \mathbf{z}), \mathbf{v})_{\Omega_t^f} + ((\mathbf{u} - \mathbf{z}) \cdot \nabla_{\mathbf{x}} \mathbf{u}, \mathbf{v})_{\Omega_t^f} \right] \\ + A((\boldsymbol{\sigma}, \mathbf{u}), (\boldsymbol{\tau}, \mathbf{v}))_{\Omega_t^f} - (p, \nabla_{\mathbf{x}} \cdot \mathbf{v})_{\Omega_t^f} + (q, \nabla_{\mathbf{x}} \cdot \mathbf{u})_{\Omega_t^f} \\ = (\mathbf{f}_f, \mathbf{v})_{\Omega_t^f} + (\mathbf{f}_s, \boldsymbol{\xi})_{\Omega^s} \quad \forall (\mathbf{v}, q, \boldsymbol{\tau}, \boldsymbol{\xi}) \in \tilde{\mathbf{U}}_t \times Q_t \times \boldsymbol{\Sigma}_t \times \tilde{\mathbf{S}},$$

where $A((\mathbf{u}, \boldsymbol{\sigma}), (\mathbf{v}, \boldsymbol{\tau})) := (\boldsymbol{\sigma}, \boldsymbol{\tau}) - 2\alpha (D_{\mathbf{x}}(\mathbf{u}), \boldsymbol{\tau}) + (\boldsymbol{\sigma}, D_{\mathbf{x}}(\mathbf{v})) + 2(1 - \alpha) (D_{\mathbf{x}}(\mathbf{u}), D_{\mathbf{x}}(\mathbf{v}))$.

We notice that there is no issue on a stress boundary condition on the interface in the monolithic scheme. However, we will need a boundary condition on the inflow portion of the interface when a partitioned scheme for (22)-(25) is considered. A streamline upwind Petrov-Galerkin (SUPG) method is applied to stabilize the constitutive equation for the fluid and the fully discretized formulation is obtained by the backward Euler method.

3. Partitioned Scheme

We consider a partitioned algorithm where the FSI problem is split into two separate subproblems, where the fluid subproblem requires a stress boundary condition in addition to the standard boundary conditions for a decoupled FSI system. The two subproblems are coupled through conditions on the interface. The most basic partitioned transmission condition is the Dirichlet-Neumann algorithm, by which the fluid subproblem is solved with the Dirichlet boundary condition,

$$\mathbf{u} = \frac{\partial \boldsymbol{\eta}}{\partial t} \quad \text{on} \quad \Gamma_{I_t},$$

and the structure subproblem is solved with the Neumann boundary condition

$$(2\nu_s D(\boldsymbol{\eta}) + \bar{\lambda}(\nabla \cdot \boldsymbol{\eta}))\mathbf{n}_s = -(\boldsymbol{\sigma} + 2(1 - \alpha)D(\mathbf{u}) - p)\mathbf{n}_f \quad \text{on } \Gamma_{I_t}.$$

There are also other transmission conditions based on the velocity and stress continuity matching conditions, but many of them require a large number of iterations to converge when fluid and structure densities are similar [8].

In our work we consider a linear combination of Dirichlet and Neumann conditions, which have shown good convergence properties with use of iterations between subproblems of Newtonian FSI systems [1, 14].

Algorithm

For $n=0,1,\dots$ do until the final time step

Initial guess of $\boldsymbol{\eta}_0^{n+1}$

for $k=0,1,\dots$ do until convergence

1. Solve the fluid subproblem with Robin boundary condition

$$\boldsymbol{\sigma}_{k+1}^{n+1} + \lambda \left(\frac{\partial \boldsymbol{\sigma}_{k+1}^{n+1}}{\partial t} \Big|_{\mathbf{y}} + (\mathbf{u}_{k+1}^{n+1} - \mathbf{z}_k^{n+1}) \cdot \nabla_{\mathbf{x}} \boldsymbol{\sigma}_{k+1}^{n+1} + g_{\beta}(\boldsymbol{\sigma}_{k+1}^{n+1}, \nabla_{\mathbf{x}} \mathbf{u}_{k+1}^{n+1}) \right) \\ - 2\alpha D_{\mathbf{x}}(\mathbf{u}_{k+1}^{n+1}) = \mathbf{0} \quad \text{in } \Omega_{t_k}^{f,n+1}$$

$$Re \left(\frac{\partial \mathbf{u}_{k+1}^{n+1}}{\partial t} \Big|_{\mathbf{y}} + (\mathbf{u}_{k+1}^{n+1} - \mathbf{z}_k^{n+1}) \cdot \nabla_{\mathbf{x}} \mathbf{u}_{k+1}^{n+1} \right) \\ - \nabla_{\mathbf{x}} \cdot \boldsymbol{\sigma}_{k+1}^{n+1} - 2(1 - \alpha) \nabla_{\mathbf{x}} \cdot D_{\mathbf{x}}(\mathbf{u}_{k+1}^{n+1}) + \nabla_{\mathbf{x}} p_{k+1}^{n+1} = \mathbf{f}_f \quad \text{in } \Omega_{t_k}^{f,n+1}$$

$$\nabla_{\mathbf{x}} \cdot \mathbf{u}_{k+1}^{n+1} = 0 \quad \text{in } \Omega_{t_k}^{f,n+1}$$

$$w_f \mathbf{u}_{k+1}^{n+1} + (\boldsymbol{\sigma}_{k+1}^{n+1} + 2(1 - \alpha)D(\mathbf{u}_{k+1}^{n+1}) - p_{k+1}^{n+1})\mathbf{n}_f \\ = \left(w_f \frac{\partial \boldsymbol{\eta}_k^{n+1}}{\partial t} - (2\nu_s D(\boldsymbol{\eta}_k^{n+1}) + \lambda(\nabla \cdot \boldsymbol{\eta}_k^{n+1}))\mathbf{n}_s \right) \circ \Psi_{t_k}^{-1} \quad \text{on } \Gamma_{I_{t_k}^{n+1}}.$$

2. Solve the structure subproblem with the Robin boundary condition

$$\rho_s \frac{\partial^2 \boldsymbol{\eta}_{k+1}^{n+1}}{\partial t^2} - 2\nu_s \nabla \cdot D(\boldsymbol{\eta}_{k+1}^{n+1}) - \bar{\lambda} \nabla(\nabla \cdot \boldsymbol{\eta}_{k+1}^{n+1}) = \mathbf{f}_s \quad \text{in } \Omega^s$$

$$w_s \frac{\boldsymbol{\eta}_{k+1}^{n+1}}{\Delta t} + (2\nu_s D(\boldsymbol{\eta}_{k+1}^{n+1}) + \lambda(\nabla \cdot \boldsymbol{\eta}_{k+1}^{n+1}))\mathbf{n}_s \\ = (w_s \mathbf{u}_{k+1}^{n+1} - (\boldsymbol{\sigma}_{k+1}^{n+1} + 2(1 - \alpha)D(\mathbf{u}_{k+1}^{n+1}) - p_{k+1}^{n+1})\mathbf{n}_f) \circ \Psi_{t_k}^{n+1} \quad \text{on } \Gamma_{I_0}.$$

3. Update $\Gamma_{I_{t_k}^{n+1}}, \mathbf{z}_k^{n+1}, \Psi_{t_k}^{n+1}$ using $\boldsymbol{\eta}_{k+1}^{n+1}$.

The algorithm presented above applies the general Robin-Robin boundary condition, where w_f, w_s are combination parameters for the transmission conditions. With an appropriate choice of w_f and w_s , we can obtain mixed schemes such as Dirichlet-Neumann, Dirichlet-Robin, Robin-Neumann etc. In our numerical experiments presented in the next section, we use the optimal values of parameters analyzed in [14].

4. Numerical Test

4.1. Convergence Test. The viscoelastic fluid subproblem of the algorithm requires an appropriate stress boundary condition for the inflow portion of boundary. In our setting, the inflow portion consists of both the inlet Γ_{inlet} and the inflow portion (when $\mathbf{u} \cdot \mathbf{n} < 0$) on the deformable interface (Figure 2).

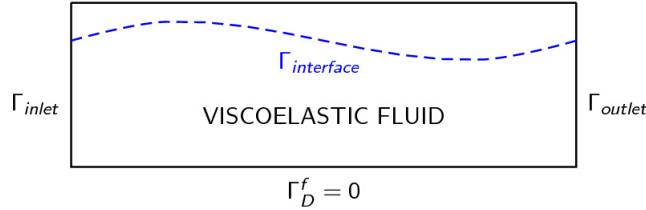


FIGURE 2. Viscoelastic Fluid Boundary.

Three different strategies regarding the stress boundary condition are considered for numerical approximations:

- (1) monolithic scheme: no stress boundary condition is imposed on the inflow portion of the interface since the interface terms are canceled in the monolithic formulation;
- (2) decoupled scheme with the do-nothing stress boundary condition: no stress boundary condition is imposed on the inflow portion of the interface;
- (3) decoupled scheme with the Dirichlet stress boundary condition: the inflow stress boundary condition is imposed using the exact solution.

We perform the convergence test for both monolithic and partitioned algorithms. Since we are interested in convergence outcomes of the FSI problem, we make the assumption that the system has infinitesimal displacements of the fluid domain and the structure, but with non-negligible velocity at the interface. Parameters chosen for the simulations are: $\rho_f = 1/0.35$, $\rho_s = 1.9$, $\beta = 0$, $\alpha = 0.5$, $w_s = 31.83$, $w_f = 722.55$, $\nu_s = 3$ and $\bar{\lambda} = 4.5$. The splitting parameters w_s, w_f for the Robin-Robin condition are chosen based on the result in [14].

Initial conditions, body forces, and boundary conditions are appropriately given such that the exact solutions on the computational domain $\Omega^f = [0, 1] \times [0, 1]$ and $\Omega^s = [0, 1] \times [1, 1.2]$ are

$$\begin{aligned} \mathbf{u} &= \begin{bmatrix} \cos(x+t)\sin(y+t) + \sin(x+t)\cos(y+t) \\ -\sin(x+t)\cos(y+t) - \cos(x+t)\sin(y+t) \end{bmatrix}, \\ p &= 2(\sin(x+t)\sin(y+t) - \cos(x+t)\cos(y+t)) + 2\nu_s \cos(x+t)\sin(y+t), \\ \boldsymbol{\sigma} &= \begin{bmatrix} \sigma_{11} & 0 \\ 0 & \sigma_{22} \end{bmatrix}, \quad \sigma_{11} = \sin(x+t)\sin(y+t) + \cos(x+t)\cos(y+t), \\ &\quad \sigma_{22} = -\sigma_{11}, \\ \boldsymbol{\eta} &= \begin{bmatrix} \sin(x+t)\sin(y+t) \\ \cos(x+t)\cos(y+t) \end{bmatrix}. \end{aligned}$$

The finite element pair $(\mathbb{Q}_2, \mathbb{Q}_1)$ is used to solve the fluid equations, while $\mathbb{Q}_2, \mathbb{Q}_1$ finite elements are used for the structure displacement and the discrete ALE mapping, respectively. Errors are computed over one time step starting from $t = 0.1$ with decreasing h and $\Delta t = 10^{-5}$.

In this test, we observe expected convergence rates by both the monolithic and decoupled schemes. However, we note that optimal convergence rates are lost if no stress boundary condition is imposed for the decoupled scheme. Considering these results, we investigate the effect of stress boundary conditions in a physical setting in the following simulation.

4.2. Hemodynamic simulation. The experiments presented in this section consist of simulating a viscoelastic FSI system with various Weissenberg numbers and

TABLE 1. Fluid convergence outcomes for monolithic viscoelastic FSI.

| h | $\ \mathbf{u}^n - \mathbf{u}^{true}\ _{L^2}$ | Rate | $\ \mathbf{u}^n - \mathbf{u}^{true}\ _{H^1}$ | Rate | $\ \boldsymbol{\sigma}^n - \boldsymbol{\sigma}^{true}\ _{L^2}$ | Rate |
|------|--|------|--|------|--|------|
| 1/8 | 4.739e-004 | - | 5.016e-003 | - | 4.957e-003 | - |
| 1/16 | 6.437e-005 | 2.88 | 1.481e-003 | 1.76 | 1.641e-003 | 1.86 |
| 1/32 | 8.159e-006 | 2.98 | 3.996e-004 | 1.89 | 4.189e-004 | 1.97 |
| 1/64 | 9.782e-007 | 3.06 | 9.852e-005 | 2.02 | 1.040e-004 | 2.01 |

TABLE 2. Convergence outcomes for the partitioned scheme with no stress boundary condition.

| h | $\ \mathbf{u}^n - \mathbf{u}^{true}\ _{H^1}$ | Rate | $\ \boldsymbol{\sigma}^n - \boldsymbol{\sigma}^{true}\ _{L^2}$ | Rate |
|------|--|------|--|------|
| 1/8 | 6.688e-003 | - | 6.830e-003 | - |
| 1/16 | 1.496e-003 | 2.16 | 1.684e-003 | 2.03 |
| 1/32 | 3.953e-004 | 1.92 | 4.181e-004 | 2.01 |
| 1/64 | 1.378e-004 | 1.51 | 1.341e-004 | 1.64 |

TABLE 3. Convergence outcomes for the partitioned scheme with Dirichlet stress boundary condition.

| h | $\ \mathbf{u}^n - \mathbf{u}^{true}\ _{H^1}$ | Rate | $\ \boldsymbol{\sigma}^n - \boldsymbol{\sigma}^{true}\ _{L^2}$ | Rate |
|------|--|------|--|------|
| 1/8 | 5.503e-003 | - | 5.037e-003 | - |
| 1/16 | 1.057e-003 | 2.38 | 1.143e-003 | 2.14 |
| 1/32 | 2.698e-004 | 1.97 | 3.063e-004 | 1.90 |
| 1/64 | 6.561e-005 | 2.04 | 7.397e-005 | 2.05 |

comparing the effects of different stress boundary conditions on fixed and moving inflow boundaries. We consider a blood flow problem reported in [22, 27], where modeling parameters in the structure equation are consistent with blood flow in a human body. The reference domain for the fluid subsystem has height 1 cm and length 6 cm. The structure domain has height 0.1 cm and length 6 cm. The den-

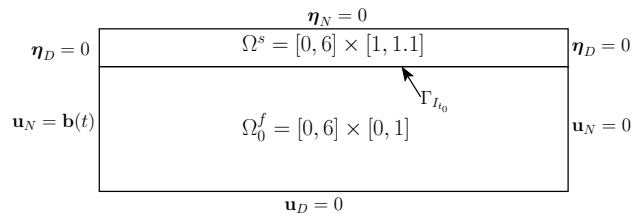


FIGURE 3. Domain and boundary conditions for numerical experiment.

sity of the structure, ρ_s , is 1.1 g/cm³. The Young's Modulus of the structure, E , is 3×10^6 dyne/cm², and its Poisson ratio, r , is 0.3. The Lamé parameters λ and ν_s are defined as in (6). The remaining parameters are the same as in the convergence test.

A force $\mathbf{b}(t)$ is applied to the left fluid boundary (Fig. 3) at t sec, where

$$\mathbf{b}(t) = \begin{cases} (-10^3(1 - \cos \frac{2\pi t}{0.25}), 0) \text{ dyne/cm}^2, & t \leq 0.025 \\ (0, 0), & 0.025 < t < T. \end{cases}$$

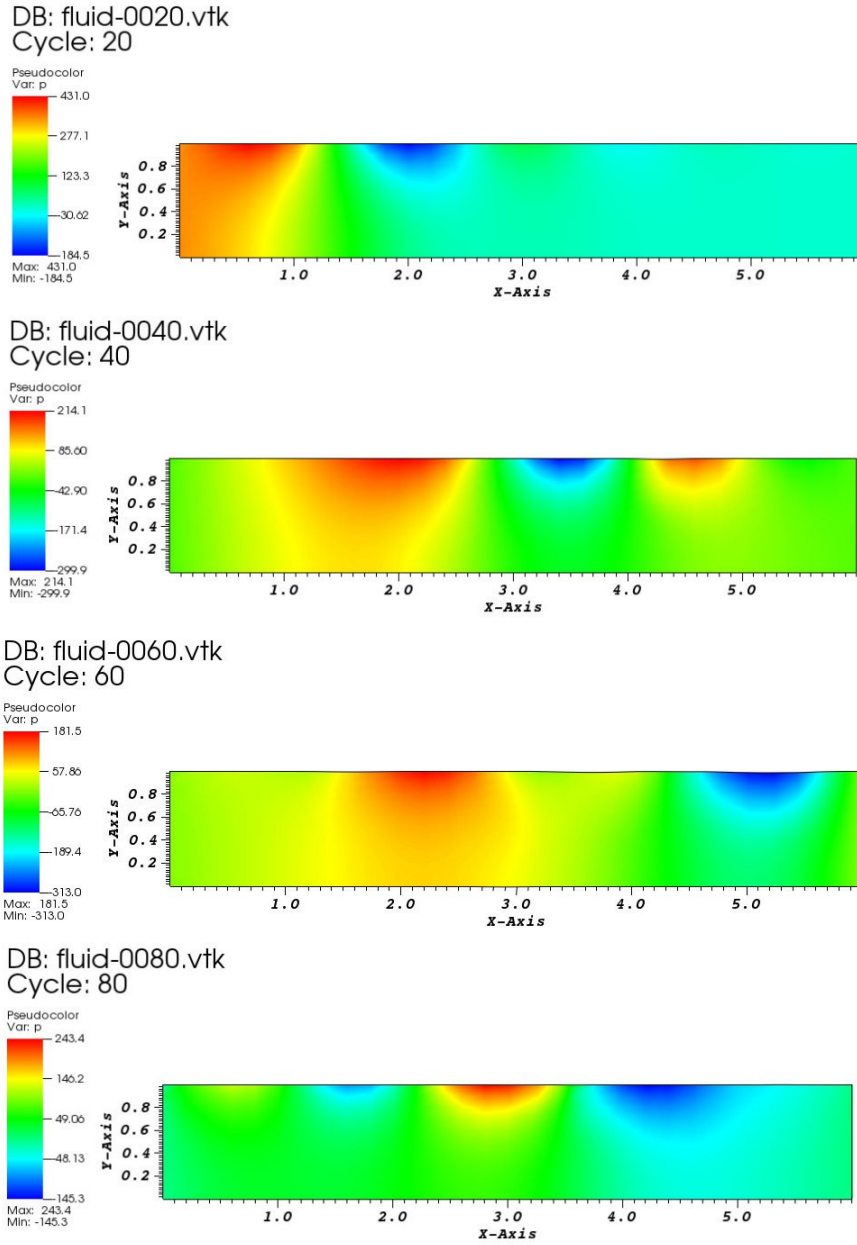
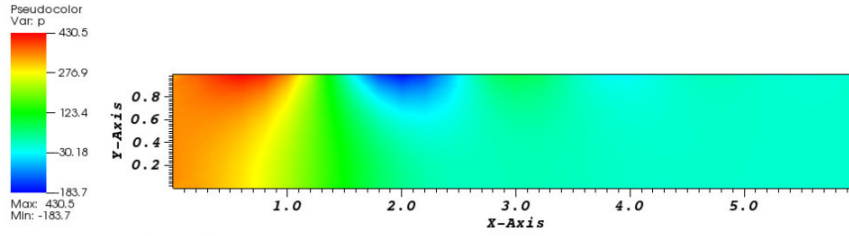


FIGURE 4. Pressure profile on the fluid domain with $\lambda = 0.9$.

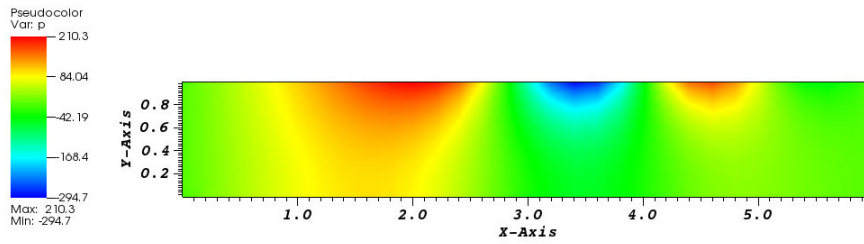
The function $\mathbf{b}(t)$ defines the stress on the inlet denoted by \mathbf{u}_N . For numerical tests, we impose the Neumann condition on both the inflow and outflow boundaries as in the references above. For any fixed time, the constitutive equation (1) could be reduced to

$$(27) \quad \boldsymbol{\sigma} + \lambda(\mathbf{u} \cdot \nabla \boldsymbol{\sigma} + g_\beta(\boldsymbol{\sigma}, \nabla \mathbf{u})) - 2\alpha D(\mathbf{u}) = \mathbf{0} \quad \text{in } \Omega_t^f.$$

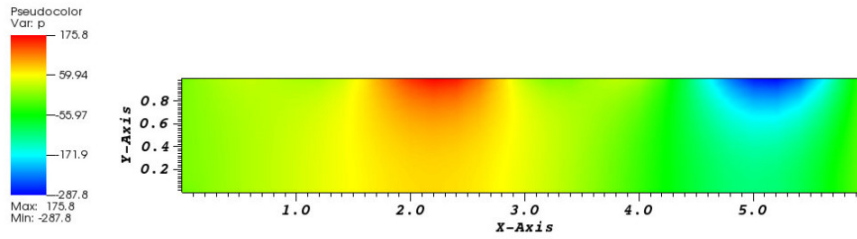
DB: fluid-0020.vtk
Cycle: 20



DB: fluid-0040.vtk
Cycle: 40



DB: fluid-0060.vtk
Cycle: 60



DB: fluid-0080.vtk
Cycle: 80

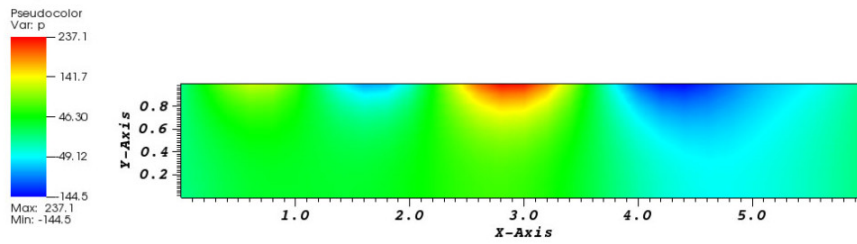


FIGURE 5. Pressure profile on the fluid domain with $\lambda = 0.06$.

Along the fixed inflow boundary on the left, the boundary condition for stress could be approximated by the steady-state constitutive equation of (27) as

$$(28) \quad \sigma_{11} = \frac{-\alpha\lambda(\beta + 1)u_{1,y}^2}{(\beta^2 - 1)\lambda^2 u_{1,y}^2 - 1},$$

$$(29) \quad \sigma_{12} = \frac{-\alpha u_{1,y}}{(\beta^2 - 1)\lambda^2 u_{1,y}^2 - 1},$$

$$(30) \quad \sigma_{22} = \frac{-\alpha\lambda(\beta - 1)u_{1,y}^2}{(\beta^2 - 1)\lambda^2 u_{1,y}^2 - 1},$$

where $u_{1,y} = \frac{\partial \mathbf{u}_1}{\partial y}$ is computed using the solution of the previous iteration step, \mathbf{u}_k^{n+1} [17]. Also, along the moving inflow boundary portion of the interface, we use the previous time step solution σ^n for the stress boundary condition, and we use homogeneous Dirichlet or Neumann boundary conditions for all other boundaries (Fig. 3). We expect no inflow of the fluid along the interface until the fluid domain starts to shrink after being maximally expanded due to the force \mathbf{b} . Therefore, no stress boundary condition is needed until that time because σ should be computed as one of the unknown functions. The volume force for the fluid and structure are $\mathbf{f}(t) = (0, 0)$ dyne/cm², and the simulation begins at rest.

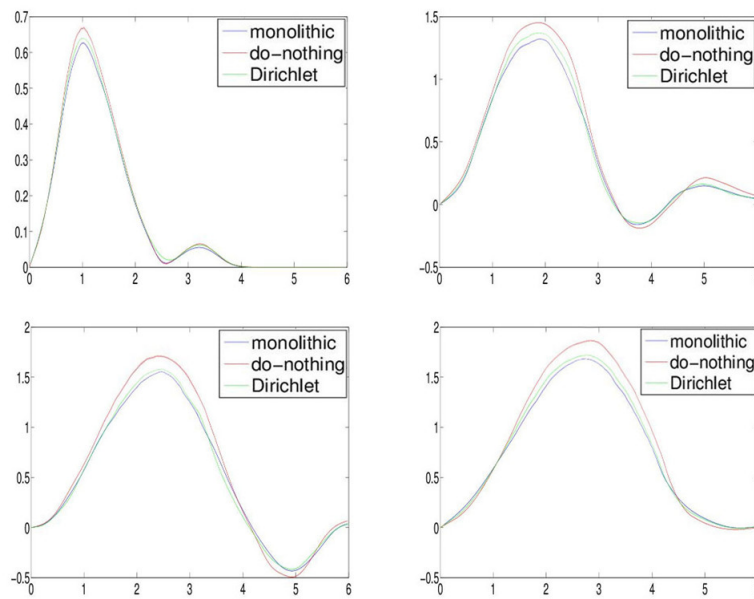


FIGURE 6. Structure displacement at $t=0.02, 0.04, 0.06, 0.08$ s with $\lambda = 0.9$.

The first test is performed with the Weissenberg number $\lambda = 0.9$. Figure 4 presents the pressure profile given by the partitioned algorithm with the Dirichlet stress boundary condition imposed on the inflow portion through a sequence of increasing times $t=0.02, 0.04, 0.06, 0.08$ s.

The corresponding vertical structure displacements (scaled by 10) given by the different schemes are compared in Figure 6. Since the monolithic scheme does not have the stress boundary issue on the interface, we compare results given by the partition scheme with and without the Dirichlet stress boundary condition against results given by the monolithic scheme. The difference among the three cases is obvious from the graphs, and we observe that the partition scheme outcome is improved with the Dirichlet stress boundary condition imposed.

In order to investigate the effects of the stress boundary condition for a fluid close to being Newtonian, we do similar experiments for a smaller Weissenberg number $\lambda = 0.06$, which is used to simulate blood flow in [26, 28]. The corresponding pressure profile is presented in Figure 5, where a similar pattern to Figure 4 is observed. We also notice that the pressure decreases with the smaller Weissenberg

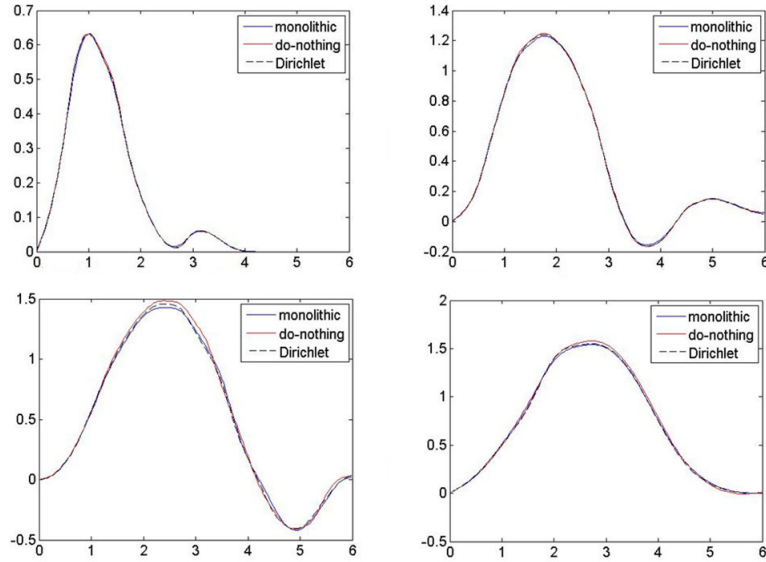


FIGURE 7. Structure displacement at $t=0.02, 0.04, 0.06, 0.08$ s with $\lambda = 0.06$.

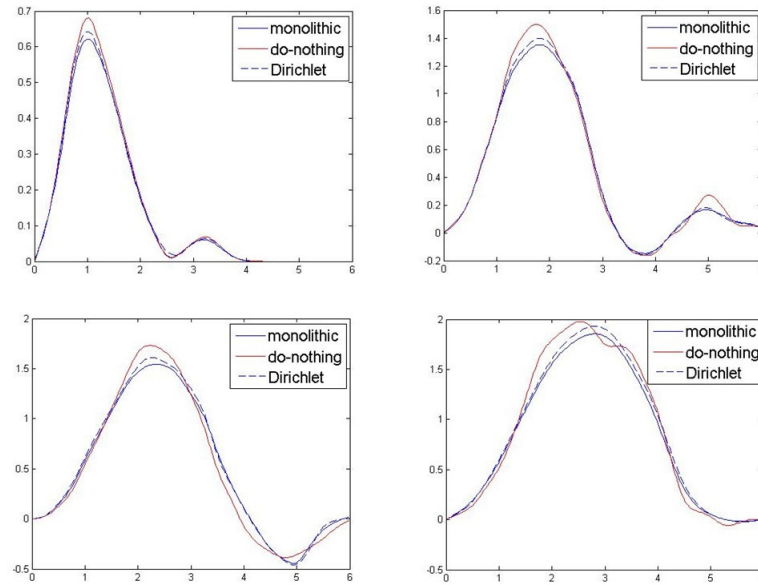


FIGURE 8. Structure displacement at $t=0.02, 0.04, 0.06, 0.08$ s with $\lambda = 2$.

number λ . For the purpose of comparison we also simulate with the relatively large Weissenberg number $\lambda = 2$, where the viscoelastic behavior is more significant.

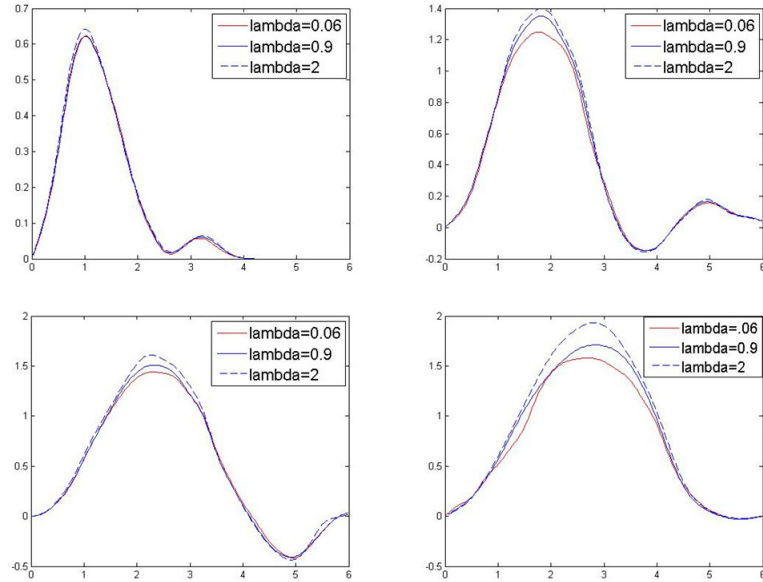


FIGURE 9. Structure displacement at $t=0.02, 0.04, 0.06, 0.08$ s with different λ values.

The structure deformations under different schemes when $\lambda = 0.06, 2$ are presented in Figure 7 and Figure 8, respectively. With the small Weissenberg number, the deformation difference is still visible but not significant. When the Weissenberg number is high, on the other hand, the difference between the algorithms is more obvious. In fact, with $\lambda = 2$, we can not obtain a steady solution without the stress condition imposed, as observed in Figure 8 where an oscillation occurs.

The vertical structure deformations under the monolithic scheme with $\lambda = 0.06, 0.9$ and 2 are compared in Figure 9. It is observed that the displacement is more significant for higher Weissenberg numbers.

5. Conclusion

We considered both monolithic and partitioned algorithms for a viscoelastic fluid-structure interaction problem. For the partition algorithm, a Robin-Robin transmission condition is applied for coupling two subproblems, where the fluid problem is approximated with and without stress boundary conditions on the inflow portion of the moving fluid boundary. Numerical tests were performed to investigate the performance of the algorithms and to compare the effects of stress boundary conditions for the viscoelastic FSI problem. The partition algorithm without stress boundary conditions failed to obtain the optimal convergence rate in the convergence test. In the blood flow simulation, the partitioned algorithm with the stress boundary condition yielded a more accurate numerical solution, in particular, when the viscoelastic property of the fluid was significant.

Acknowledgments

This research was supported by NSF under grants DMS-1418960.

References

- [1] S. Badia, F. Nobile and C. Vergara, Fluid-structure partitioned procedures based on Robin transmission conditions, *Journal of Computational Physics*, 227(14), 7027-7051, 2008.
- [2] O.K. Baskurt and H.J. Meiselman, Blood rheology and hemodynamics, *Semin. Thromb. Hemost.*, 29, 435-450, 2003.
- [3] T. Bodnár, K.R. Rajagopal and A. Sequeira, Simulation of three-dimensional flow of blood using a shear-thinning viscoelastic fluid model, *Math. Model. Nat. Phenom.*, 6, 1-24, 2011.
- [4] T. Bodnár and A. Sequeira, Numerical study of the significance of the non-Newtonian nature of blood in steady flow through a stenosed vessel, in *Advances in Mathematical Fluid Mechanics*, 83-104, 2010.
- [5] T. Bodnár, A. Sequeira and M. Prosi, On the shear-thinning and viscoelastic effects of blood flow under various flow rates, *Appl. Math. Comput.*, 217, 5055-5067, 2011.
- [6] E. Burman and M.A. Fernández, Stabilization of explicit coupling in fluid-structure interaction involving fluid incompressibility, *Comput. Methods Appl. Mech. Engrg.*, 198, 766-784, 2009.
- [7] S. Canić, A. Mikelić, and J. Tambaca, Two dimensional effective model describing fluid-structure interaction in blood flow: analysis, simulation and experimental validation, *Comptes Rendus Mécanique Acad. Sci.*, 333, 867-883, 2005.
- [8] P. Causin, J-F. Gerbeau and F. Nobile, Added-mass effect in the design of partitioned algorithms for fluid-structure problems, *Comput. Methods Appl. Mech. Engrg.*, 194, 4506-4527, 2005.
- [9] W. Chan, Y. Ding and J. Tu, Modeling of non-Newtonian blood flow through a stenosed artery incorporating fluid-structure interaction, *Anziam Journal*, 47, 507-523, 2007.
- [10] X. Chen, M. Schafer and D. Bothe, Numerical modeling and investigation of viscoelastic fluid-structure interaction applying an implicit partitioned coupling algorithm, *Journal of Fluids and Structures*, 54, 390-42, 2015.
- [11] L. Formaggia, J.F. Gerbeau, F. Nobile and A. Quarteroni, On the Coupling of 3D and 1D Navier-Stokes equations for Flow Problems in Compliant Vessels, *Comput. Methods Appl. Mech. Engrg.*, 191, 561-582, 2001.
- [12] L. Formaggia, A. Moura and F. Nobile, On the stability of the coupling of 3D and 1D fluid-structure interaction models for blood flow simulations, *Math. Mod. Numer. Anal.*, 41, 743-769, 2007.
- [13] M. W. Gee, U. Küttler and W. A. Wall, Truly monolithic algebraic multigrid for fluid-structure interaction, *International Journal for Numerical Methods in Engineering*, 85, 987-1016, 2011.
- [14] L. Gerardo-Giorda, F. Nobile and C. Vergara, Analysis and optimization of Robin-Robin partitioned procedures in fluid-structure interaction problems, *SIAM J. Num. Anal.*, 48, 2091-2116, 2010.
- [15] F. J. H. Gijen, F. N. van de Vosse and J. D. Janssen, The influence of the non-Newtonian properties of blood on the flow in large arteries: steady flow in a carotid bifurcation model, *Journal of Biomechanics*, 32, 601-608, 1999.
- [16] M. Heil, An efficient solver for the fully coupled solution of large-displacement fluid-structure interaction problems, *Comput. Methods Appl. Mech. Engrg.*, 193, 1-23, 2004.
- [17] V. Ervin, J. Howell and H. Lee, A two-parameter defect-correction method for computation of steady-state viscoelastic Fluid Flow, *Appl. Math. and Compt.*, 196, 818-834, 2008.
- [18] J. Hron, S. and Turek, A monolithic FEM/multigrid solver for an ALE formulation of fluid-structure interaction with applications in biomechanics, in *Fluid-Structure Interaction: Modeling, Simulation, Optimization*. Lecture Notes in Computational Science and Engineering, 53, 146 - 170, Bungartz, Hans-Joachim; Schafer, Michael (Eds.), Springer, 2006.
- [19] J. Janela, A. Moura and A. Sequeira, A 3D non-Newtonian fluid-structure interaction model for blood flow in arteries, *J. Comput. Appl. Math.*, 234, 2783-2791, 2010.
- [20] J. Janela, A. Moura and A. Sequeira, Absorbing boundary conditions for a 3D non-Newtonian fluid-structure interaction model for blood flow in arteries, *International Journal of Engineering Science*, 48(11), 1332-1349, 2010.
- [21] B.M. Johnson, P.R. Johnson, S. Corney and D. Kilpatrick, Non-newtonian blood flow in human right coronary arteries: steady state simulations, *Journal of Biomechanics*, 37(5), 709-720, 2004.
- [22] P. Kuberry and H. Lee, A decoupling algorithm for fluid-structure interaction problems based on optimization, *Comput. Methods Appl. Mech. Engrg.*, 267, 594-605, 2013.

- [23] H. Lee and S. Xu, The finite element error estimation for Quasi-Newtonian fluid-structure interaction problems, *ph Applied Mathematics and Computation*, 274, 93-105, 2016.
- [24] H. Lee and S. Xu, Fully discrete error estimation for a quasi-Newtonian fluid-structure interaction problem, *Computers & Mathematics with Applications*, 71(11), 2373-2388, 2016.
- [25] M. Lukáčová and A. Zaušková, Numerical modelling of shear-thinning non-Newtonian flows in compliant vessels, *Int. J. Numer. Meth. Fluids*, 56, 1409-1415, 2008.
- [26] A. Leuprecht and K. Perktold, Computer simulation of non-Newtonian effects on blood flow in large arteries, *Computer Methods in Biomechanics and Biomedical Engineering*, 4(2), 149-163, 2001.
- [27] C. M. Murea and S. Sy, A fast method for solving fluid-structure interaction problems numerically, *International Journal for Numerical Methods in Fluids*, 60(10), 1149-1172, 2009.
- [28] L. Nadau and A. Sequeira, Numerical simulations of shear dependent viscoelastic flows with a combined finite element–finite volume method, *Comput. Math. Appl.*, 53, 547-568, 2007.
- [29] A.M. Robertson, A. Sequeira and M.V. Kameneva, Hemorheology, in *Hemodynamical Flows: Modeling, Analysis and Simulation (Oberwolfach Seminars, Birkhauser)*, G.P. Galdi, R. Rannacher, A.M. Robertson, S. Turek (Eds.), 63-120, 2008.
- [30] T. Wick, Solving Monolithic Fluid-Structure Interaction Problems in Arbitrary Lagrangian Eulerian Coordinates with the deal.II Library, *Archive of Numerical Software*, 1, 2013.

Department of Mathematical Sciences, Clemson University, Clemson, SC 29634-0975
E-mail: hklee@clemson.edu and shuhanx@g.clemson.edu